Picometer-scale dynamical observations of individual membrane proteins: The case of bacteriorhodopsin

Yasuaki Okumura,[1,2,3] Toshihiko Oka,[2] Mikio Kataoka,[4] Yoshio Taniguchi,[3] and Yuji C. Sasaki[2,*]
[1]*CREST–Sasaki Team, Japan Science and Technology Corporation (JST), Tachikawa 190-0012, Japan*
[2]*Life & Environmental Science Division, SPring-8/JASRI, Mikazuki, Sayo, Hyogo 679-5198, Japan*
[3]*Department of Biomolecular Science and Technology, University of Shinshu, Ueda, Nagano 386-8567, Japan*
[4]*Graduate School of Material Science, Nara Institute of Science and Technology, Ikoma, Nara 630-0101, Japan*
(Received 5 September 2003; published 31 August 2004)

In vivo measurements of dynamical conformational changes in single biomolecules under functional conditions have had a tremendous impact on molecular and cell biology. However, even single-molecule fluorescent resonance energy transfer cannot easily monitor the intramolecular dynamics in cell systems due to shortcomings in monitoring precision. Here, we report dynamical observations of irreversible intramolecular conformational changes in a single-membrane protein [bacteriorhodopsin (BR)] using diffracted x-ray tracking. The light-driven proton pump BR is the best-characterized membrane protein. The position of BR's 35th amino acid, which is located farthest from retinal, exhibits a momentary positional jump of 0.73 ± 0.48 Å due to the expression of its function. Following that, we observed Brownian motion without the diffracted spots returning to their initial positions. The average width of this jump is about 14 times larger than that of thermal Brownian motion and agrees with estimated movements from known x-ray crystallography data. This result is an important step toward realizing *in vivo* observations of single-molecular conformational changes in membrane proteins.

DOI: 10.1103/PhysRevE.70.021917 PACS number(s): 82.37.Vb, 02.70.Ns

I. INTRODUCTION

It is important to measure the dynamic structural details of individual membrane proteins that express the function of signal transduction in cell systems. This is because it is not speculation from fragmentary or static structural information, but rather dynamical information from individual membrane proteins, that can more accurately and directly determine the detailed mechanisms that express the functions of individual membrane proteins in cell systems [1,2]. Single molecular imaging techniques using fluorescent probes (λ), which have enabled dynamical observations of single biomolecules, have proved to be valuable tools in solving many basic problems in biophysics, because these methods have been providing positional information on single molecules at an accuracy of about $\lambda/100$, far below the optical diffraction limit ($\sim\lambda/2$) [3]. Moreover, single-molecule fluorescence resonance energy transfer (single-molecule FRET), which relies on the distance-dependent transfer of energy from a donor fluorophore to an acceptor fluorophore, is one of the few tools available for measuring nanometer-scale distances and changes in distances, or both the intramolecular and intermolecular orientation between the two fluorophores, both *in vitro* and *in vivo* [4]. However, it is difficult to measure intramolecular structural changes of single proteins in membranes with single-molecule FRET due to the lack of monitoring precision and stability of the signal intensity in physiological conditions.

Diffracted x-ray tracking (DXT), a new single-molecule technique using x rays ($\lambda_{x\ ray} \sim 0.1$ nm), has been proven to be able to observe single molecular motions to a picometer-level accuracy ($\lambda_{xray}/100$) using DNA molecules [5–7]. DXT monitors the spots of diffracted x rays from individual nanocrystals that are tightly labeled with single molecules [Fig. 1(a)]. The extremely short-wavelength x rays that form the probe of this method lead to its excellent characteristics, because they enable us to observe single-molecular dynamics with extremely high accuracy. The x rays as transmitted by the probe result in actualization of the stable observations under *in vivo* conditions because x-ray diffraction is independent of physiological conditions.

In this study, we observed Brownian motions and light-driven structural changes in the *A*-*B* interhelical loop of individual bacteriorhodopsin (BR) molecules in a purple membrane (PM) using DXT with gold nanocrystals. Bacteriorhodopsin is the most extensively studied membrane protein precisely because the purple membrane is so robust to chemical treatments used in this study (Hg labeling and immobilization on the substrate using chemical coupling), which would destroy most membrane-coating proteins. Therefore, for this reason we have chosen BR.

Bacteriorhodopsin plays the role of a light-driven proton pump in a PM, which is a patch of cell membrane of *Halobacterium salinarium*. The BR passes through a series of well-characterized spectral intermediate states designated *J*, *K*, *L*, *M*, *N*, and *O*, in the order of their appearance in the cycle (photocycle), after light of wavelength around 570 nm induces isomerization of the retinal located inside the BR. A photocycle is coupled to vectorial proton transport from the cytoplasmic to the extracellular side of the PM [8–13].

In this study, we used single cystein-containing BR mutants BR S35C for the following three reasons: (i) it is known that BR S35C has nearly unperturbed photocycles

*Corresponding author. Fax: +81–79158–2512. Email address: ycsasaki@spring8.or.ip

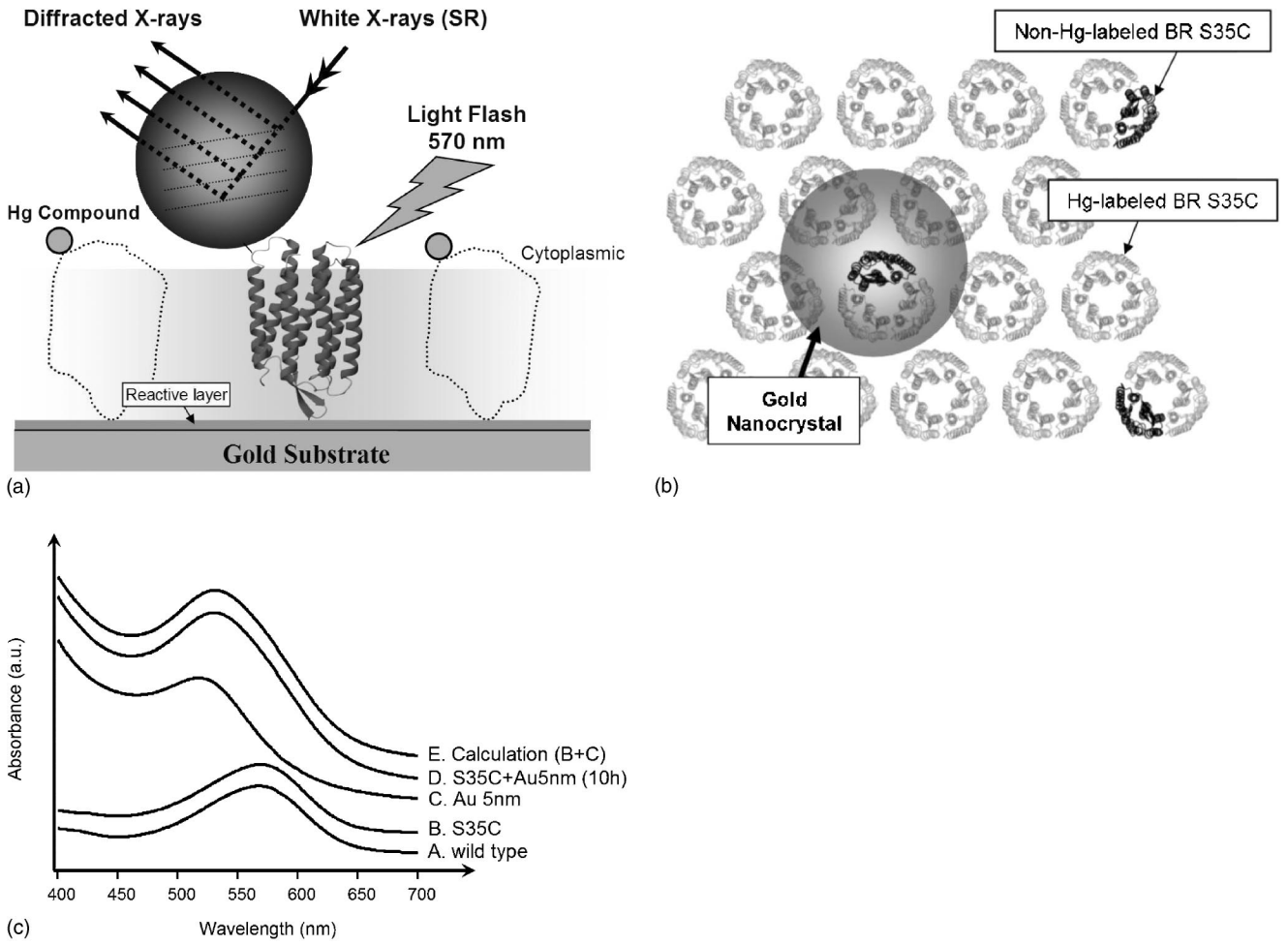

FIG. 1. Experimental designs of DXT. (a) Schematic drawing of the cross-sectional view of DXT in the case of BR S35C. DXT monitors the spots of diffracted x rays from individual nanocrystals that are tightly labeled with individual BR S35C. Samples containing the immobilized BR S35C were filled with the oxygen scavenger system (25 mM glucose, 14 mM 2-mercaptoethanol, 10 nM catalase, and 2.5 μM glucose oxidase) in 50 mM MOPS (pH 7.0). (b) Schematic illustration showing the top view of DXT using BR S35C. The 1:1 ratio of BR molecules to nanocrystals is possible because of the Hg compound (PCMB) first labeled with excess sulfhydryl groups in BR S35C. BR S35C-labeled PCMB is shown in silver, and nonlabeled BR S35C is shown in black; that is, black BR S35C can be linked to gold nanocrystals. (c) Optical-absorption spectrum of wild-type BR (*A*), BR S35C (*B*), colloidal gold (*C*), colloidal gold-labeled BR S35C (*D*), and calculated spectra (*B*+*C*) (*E*). Absorption maximum of (*A*) or (*B*) is 568 nm.

compared with wild-type BR [13]; (ii) cystein residues that link ~15-nm-diam gold nanocrystals are located in the *A*-*B* interhelical loop on the outside of the purple membrane (the cytoplasmic side) [Fig. 1(a)]; and (iii) we expect that labeling the 35th amino acid residue with gold nanocrystals using chemical coupling would have barely any influence on expressions of the BR molecule's function. This is because that position is located in the position most remote from the retinal inside BR. In addition, DXT is appropriate to observe the small motions in a single biomolecule because of its high accuracy. In other words, DXT could not observe the entire process of large motions such as are indicated by motor protein (e.g., F_1-ATPase). For the above reasons, we first focused attention on the 35th amino acid.

II. INSTRUMENTATION FOR DXT

The DXT experiments were conducted in the white x-ray mode of beamline BL44B2 (RIKEN Structural Biology II, SPring-8, Japan) [14]. The x-ray energy range was 7–30 keV, and the focused x-ray beam was 0.2 mm (horizontal) $\times$0.2 mm (vertical). We estimated the photon flux at the sample position (0.2 mm$\times$0.2 mm) to be 4×10^{13} photons/s. The diffraction spots from nanocrystals were recorded by a CCD camera (Hamamatsu Photonics, C4880-82) in combination with a 6-in. x-ray image intensifier (Hamamatsu Photonics, V5445P). With this system, not all diffracted spots from all gold nanocrystals presented within the detection area (0.2 mm$\times$0.2 mm) can be monitored because there are some restrictions on diffraction conditions (such as the orientation of individual labeled gold nanocrystals and the size of the detector), and diffraction spots from many imperfect gold nanocrystals are not monitored. The specimen-to-detector distance was 100 mm. In this system, the rotating motions of nanocrystals linked to individual molecules could be detected in angle ranges of 2θ=0–640 mrad. We used a xenon flash lamp (SA200E,

Eagle-shoji) with a band-pass filter ($520 < \lambda < 580$ nm) to excite the sample enough to initiate the BR photocycle.

III. FABRICATION OF GOLD NANOCRYSTALS

To operate single-molecule detection systems using x rays, it is necessary to fabricate dispersed nanocrystals and observe their diffraction spots [15]. We used gold nanocrystals fabricated by vacuum epitaxial evaporation on a NaCl (100) surface [16]. Nanocrystals are detached from the NaCl (100) substrate by dissolving the substrate in an aqueous solution. We confirmed the diameters of these crystals in aqueous solution to be 10–15 nm by dynamic light scattering and atomic force microscopy. Moreover, fabricated gold nanocrystals generated the diffraction spots from only the (100) direction because these crystals were grown epitaxially on the NaCl (100) substrate [16–18]. Therefore, one nanocrystal can generate at most two (one pair) diffraction spots. We can easily find these spots from these nanocrystals presented in aqueous solutions, because motions of these spots are perfectly synchronized all the time on the screen. In addition, there is no possibility that one diffraction spot is generated from multiple nanocrystals because these spots move randomly all the time. Even if this were possible, we could easily distinguish the overlapped diffraction spots because DXT can quantitatively measure x-ray intensity of diffracted spots from nanocrystals [5]. Therefore, observed single diffraction spots come from single nanocrystals.

IV. LABELING OF BR S35C PROTEIN ONTO THE SUBSTRATE

To observe the motions of single BR S35C in a membrane, we immobilized PMs on the amorphous gold substrate with a cross-linking reagent (succinimidayl 6-[3-(2-pryidyldithio)-propionamido]hexanoate: LC-SPDP, Pierce Co., Ltd.) in 50 mM HEPES (pH 8.0) for 6 h at 25°C. This cross-linking reagent containing pyridyl disulfide residue and *N*-hydroxysuccinimide residue ensured that we could label the gold substrate surface with specific amino acids (Lys, Ser, or Tyr) of BR S35C in PMs [19,20]. When the extracellular side of the PM reacts with the substrate surface, the cytoplasmic side, which contains the only one sulfhydryl group (35th amino acid), can be labeled with gold nanocrystals.

V. LABELING OF GOLD NANOCRYSTALS TO BR S35C

One of the most important points required for the DXT technology to work is the necessity for single BR S35C molecules to react with single nanocrystals [Fig. 1(b)]. In order to achieve this, immobilized BR S35C on the substrate was first labeled with a mercury compound [*p*-chloromercuribenzoic acid (PCMB)] in 50 mM phosphate buffer pH 7.0 for 2 h at room temperature, which specifically reacts with sulfhydryl groups and allows high occupancy [8]. Next, gold nanocrystals were labeled with sulfhydryl groups in BR S35C.

Assuming the purple membranes (PM) are fully immobilized on the surface of the substrate, the number of gold nanocrystals, which are mounted on the substrate, is less than 0.1% of that of BR S35C (the number of BR S35C is 1.5×10^{12}; the number of gold nanocrystals is 4.0×10^{9}). When the solution including gold nanocrystals was directly mounted on adsorbed PM, we monitored many diffraction spots from gold nanocrystals on the one screen. Moreover, it is expected that a single nanocrystal will be labeled with seven or eight proteins with cysteine sites because the size of the nanocrystal is about three times larger than each BR molecule. PCMB reaction with sulfhydryl groups in BR S35C led to a significant decrease in the number of observed diffraction spots. When the incubation time of PCMB was 2 h, we monitored only a few spots on one screen, and when the incubation time was 3 h we could not detect the diffraction spot as well as in the case of using wild-type BR, which does not have sulfhydryl groups on the protein surface. This result shows that the nanocrystals react with BR S35C using covalent binding through sulfhydryl groups in BR 35C.

Furthermore, in PCMB treatment samples (PCMB reaction time 2 h), we monitored that the diffracted spots from nanocrystals displayed the positional jump by light irradiation (~570 nm) due to the conformational changes of BR S35C [Fig. 2(a)]. However, in the case of nontreatment of PCMB, the movements of diffraction spots were momentarily stopped by light irradiation (data not shown). This result indicates that single nanocrystals, which are bound to multiple BR S35Cs, are not able to move because these BRs exhibit structural change toward several different directions at a time. An increase in PCMB reaction time led to a decrease in the number of stopped diffraction spots and an increase in that of jumped diffraction spots. In other words, only when a single nanocrystal was bound to a single BR molecule could we observe the reproducible positional jumps of diffraction spots.

These results thus indicate that when PCMB incubation time was 2 h, the single nanocrystal was expected to react with a BR S35C molecule using covalent bonding.

VI. EXPERIMENTAL RESULTS

Through optical-absorption methods, we ascertained that the environment around the retinal of gold-labeled BR S35C had a structure unperturbed from wild-type BR. Figure 1(c) shows the absorption spectra of (*A*) wild-type, (*B*) BR S35C, (*C*) colloidal gold (5 nm in diameter, nanoprobes), which specifically reacts with sulfhydryl groups at the highest efficiency, and is dispersive at high concentrations in the aqueous solution (5.0×10^{13} units/mL), (*D*) colloidal gold-labeled BR S35C at the equimolar concentration of 50 mM MOPS, pH 7.0, 25°C for 10 h, and (*E*) calculated spectra (*B*+*C*). Absorption spectra of wild-type BR agree closely with that of BR S35C (peak wavelength 568 nm), and the obtained absorption spectra of colloidal gold-labeled BR S35C agree well with the calculated spectra.

Figure 2(a) shows sequential images at 36-ms intervals of the single diffracted spot from the gold nanocrystal labeled with a single BR S35C. The exposure time of each image

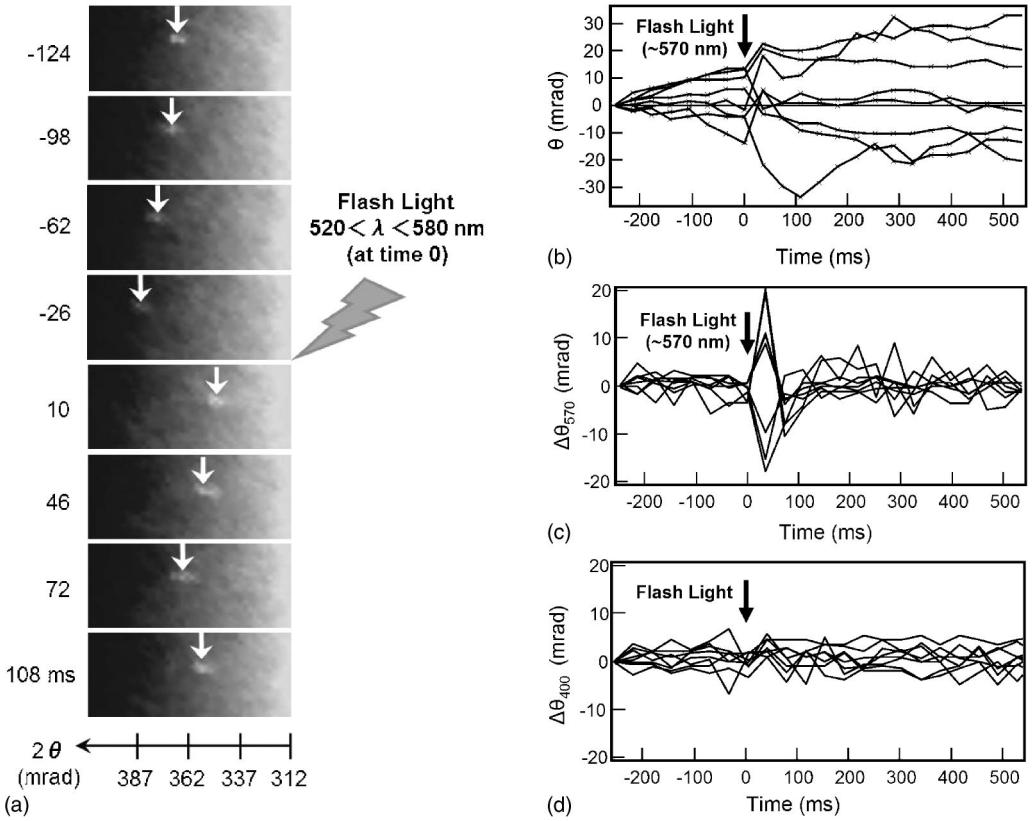

FIG. 2. Real-time tracking of diffracted spots and the view of positional jump of BR S35C due to light irradiations (~570 nm). (a) DXT images of diffracted spots from the gold nanocrystal linked to individual BR S35Cs. The arrows show the positions of a diffracted spot at 36-ms intervals. The significantly positional jump of a diffracted spot was observed by flashing light at a particular wavelength. (b) These trackings, which are randomly chosen from 70 observed spots, were measured from DXT images. The arrow shows the light irradiation at time 0 for expressing function of BR S35C. (c), (d) Displacement of θ ($\Delta\theta_{570}$ and $\Delta\theta_{400}$) of observed diffracted spots with ~570-nm and ~400-nm lights.

was 2.5 ms and the sample temperature was fixed at 8°C with a cryostat using liquid nitrogen. The low-angle (right) sides show higher background signals because the direct beam's scattering effect cannot be completely covered by the beam stopper. The initial positions of diffracted spots at −124 ms and directions of positional jumps of diffracted spots at 10 ms are random, because there was no control over the orientation of BR S35C immobilized on the substrate and the plane direction of gold nanocrystals labeled with BR S35C. The intensities of the diffracted spot in all images are constant because x rays are hardly affected at all by chemical environments, which is one of the DXT method's greatest advantages.

Before light irradiation at time 0, the diffracted spot moved toward a higher diffraction angle. Immediately after the light irradiation (570 nm), at 10 ms, we monitored the significant positional jump ($\Delta\theta$=18.1 mrad) of the diffraction angle (2θ) to the low-angle direction. Following that, we observed that the fluctuations in the diffracted spots were identical to their respective states before the light irradiation, without returning to their initial position at −124 ms.

Figures 2(b) and 2(c) show real-time tracking (θ) and displacement ($\Delta\theta$) of the eight diffracted spots taken at 36-ms intervals, respectively. The spots all move randomly, and their momentary positional jumps due to light irradiation at time 0 were performed within 10 ms. None of the diffracted spots returned to their starting positions after light irradiation within the measuring time (540 ms) and beyond the time shown, although by carrying out spectroscopic experiments under the same conditions, the excitation of the retinal in the BR protein has been confirmed to return to its initial state within about 100 ms [12,13]. Furthermore, when the same position flashed the light again after about 5 s from the first flash, diffracted spots exhibited the positional change of the same value with the first flash. This time interval is a minimum time between the first and second flashes of the xenon flash lamp. This result indicates that the retinal site would return to the initial state, although the diffracted spots do not return to the initial position before the light irradiation.

To consider the dependence of a diffracted spot's monitored positional jump on the irradiated light's wavelength, we conducted experiments to observe the effect on irradiated BR S35C using wavelengths ($350<\lambda<430$ nm and $\lambda>700$ nm) outside BR's absorption range. Results confirmed that positional changes due to ~400-nm or ~700 -nm light irradiation were not observed [Fig. 2(d)]. Therefore, the strikingly positional jumps in Fig. 2(c) indicate dependence on the irradiated light's wavelength ($520<\lambda<580$ nm) and this phenomenon is due to the photocycle of BR S35C. However, at present it cannot be denied with absolute certainly that these motions may be a result of

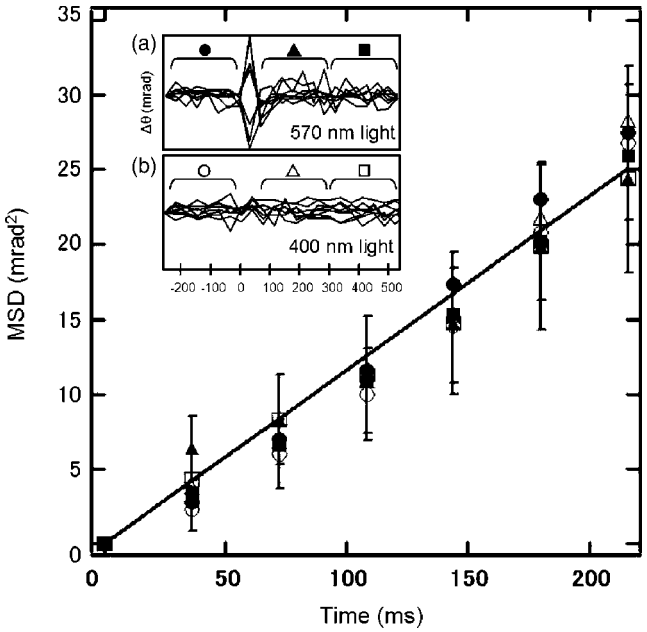

FIG. 3. Curves of mean-square displacement ($\Delta\theta^2$) of nanocrystals as a function of time interval Δt among three regions for analyses of Brownian motions. Two insets show Figs. 2(c) and 2(d). Six symbols represent the experimental results for 70 diffracted spots, while solid curves show the theoretical curve fittings.

thermal expansion of BR itself, due to absorption of the light [21].

The observed positional jumps completed within 10 ms at 8 °C are averaged at $\Delta\theta_{\max}=14.6\pm9.7$ mrad across the 70 spots. This error value of $\Delta\theta_{\max}$ may be caused by immobilization of BR S35C on the substrate, the labeling of gold nanocrystals with BR S35C, or individual adsorbed BR S35C characteristics. To clarify the understanding of real space, the rotating angles of $\Delta\theta_{\max}$ occurring at momentary structural changes are regarded as translational motions ($\Delta\sigma_{\max}$) on a two-dimensional flat surface. Assuming the height of BR S35C to be 5.0 nm, the observed moving distance in DXT is estimated to be $\Delta\sigma_{\max}=0.73\pm0.48$ Å [5].

We analyzed Brownian motions of the *A*-*B* interhelical loop in BR S35C before and after light irradiation. Figure 3 shows the relations between mean-square displacement (MSD) ($\Delta\theta^2$) of the observed spots and the time interval Δt among three regions. Six symbols in Fig. 3 show the experimental results from 70 diffracted spots, while a solid curve shows the theoretical curve fitting. The two insets in Fig. 3 show the displacements ($\Delta\theta$) of diffracted spots taken at 36 -ms intervals with (a) ~570-nm light [Fig. 2(c)] and (b) ~400-nm light [Fig. 2(d)] at time 0.

Filled and open circles in Fig. 3 show the results of statistical analysis for 250 ms before light irradiation. Triangles in Fig. 3 show the results for 250 ms after light irradiation, while squares in Fig. 3 show the results for 250 ms after the triangles data. Theoretical curve fittings of these six MSD plots show that they are linear with equivalent slopes. In a simple Brownian motion, the $(\Delta\theta^2)-\Delta t$ plots are linear, with slopes of $4D$, where D is the diffusion coefficient (mrad^2/s) in rotational motion. Simple Brownian motion can be expressed as $(\Delta\theta^2)=4D_{\text{linear}}(\Delta t)$[5,22]. From these curve fittings, we obtained the values of the diffusion constant $D=27.8\pm1.0$ mrad^2/s and these MSD curves show the simple Brownian motion. This result indicates that the motions of the *A*-*B* interhelical loop in BR S35C are assigned to simple Brownian motion, even though BR S35C was immobilized on the substrate.

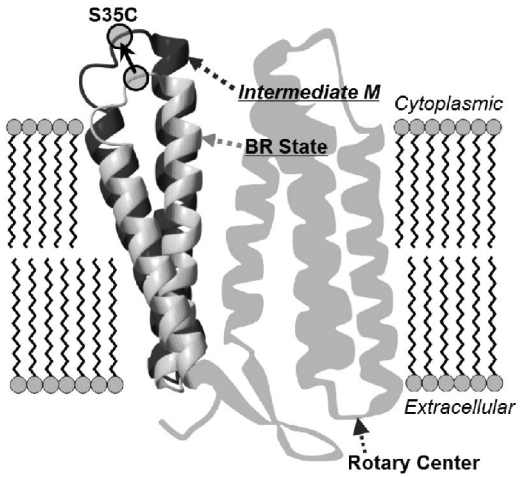

FIG. 4. Positional change of BR S35C by light irradiation (~570 nm). The BR structure is the BR state (silver, PDB ID: 1C8R) superimposed onto intermediate *M* (black, PDB ID: 1C8R). The solid arrow shows the positional change of BR S35C between the two states with the 131st amino acid as the center of rotation.

VII. DISCUSSION

According to related works on spectroscopic experiments [11,12], the rise time at intermediate *M* is expected to be less than 10 ms 8 °C. Therefore, positional jumps shown in Figs. 2(a) and 2(b) are assigned to the conformational change of BR state → intermediate *M* (BR→*M*). To confirm this assignment, two PDB files (PDB ID: 1C8R, 1C8S) which are structural data of BR state and intermediate *M*-determined x-ray crystallography were superposed upon each other (Fig. 4). DXT is used to monitor rotational motions (not translational ones) with high accuracy; therefore, the position of the rotating center is an important factor for DXT [5]. In this system, the rotating center [Fig. 1(a)] is assigned to an amino acid residue (64th, 79th, 129th, 131st, 132nd, or, 133rd amino acid), which contains amino or hydroxyl groups and reacts with the reactive layer on the substrate, which in this case is the extracellular side of the BR proteins. According to the result of the superposition of PDB files, the average expected value (~19.3 mrad) of momentary positional change between the rotating center and the 35th amino acids during the BR →*M* transition closely agreed with that ($\Delta\theta_{\max}=14.6\pm9.7$ mrad) obtained by our DXT experiments.

According to the diffusion constant ($D=27.8\pm1.0$ mrad^2/s) obtained from MSD curve fittings in Fig. 3, the average movable angle for 10 ms is about 1.1 mrad. Therefore, the size of the observed positional jump

(14.6 mrad/10 ms) is about 14 times larger than that of before or after light irradiation. Additionally, we estimated the shortest time for the diffracted spots to return to their initial positions [the rise time of the intermediate $M \rightarrow \mathrm{BR}$ state ($M \rightarrow \mathrm{BR}$)] after the positional jump due to light irradiations to be approximately 1.9 s. According to related works [12,13], the rise time of $M \rightarrow \mathrm{BR}$ is completed within about 100 ms under our conditions, indicating that the retinal and its surrounding structures that affect the spectroscopic experiments can return to their initial state for about 100 ms. However, the *A*-*B* interhelical loop did not return to its initial position during the measuring time and beyond the time shown after light irradiation.

Consequently, although the rise time of the $\mathrm{BR} \rightarrow M$ reaction obtained by spectroscopic experiments is in fair agreement with that obtained by the DXT experiment, the rise time of $M \rightarrow \mathrm{BR}$ disagrees with that of the DXT experiment. Dynamical observations of intramolecular conformational changes in single BR S35C using DXT indicate one possibility in both $\mathrm{BR} \rightarrow M$ and $M \rightarrow \mathrm{BR}$ as follows: the propagated motion from the retinal toward the *A*-*B* interhelical loop by retinal photo isomerization causes momentary positional jumps of the *A*-*B* interhelical loop. However, in the $M \rightarrow \mathrm{BR}$ reaction, the motion that returns it to BR's initial state is not propagated to the *A*-*B* interhelical loop, even though the retinal returns to its initial state. Furthermore, diffracted spots move all the time due to Brownian motions, regardless of the light flash. Therefore, it is expected that there is flexibility of the initial position itself of the *A*-*B* loop.

Here we discuss the effect of labeled nanocrystals. The labeling of nanocrystals does influence the motion of the BR protein; however, according to the Navier-Stokes equation, the dominant factor in the movements of the nanocrystals is not the mass (gravity) but the viscosity and the steric hindrance of the size of the nanocrystals. Currently, we can measure the dynamics of many proteins (for example, myosin [6], actin [23], chaperon, and channel protein) by employing the using gold nanocrystals used in this work. Consequently, we confirmed that each movement of nanocrystals, which are labeled with these different proteins, depends on each protein. This result indicates that motions of each protein can be propagated to the nanocrystals. Additionally, in order to visualize motions of an individual biomolecule, there are many studies using various nanoparticles labeled with an objective molecule [24–26]. In particular, Yasuda *et al.*, showed the rotary motion of a single molecule of F_1-ATPase labeled with colloidal gold (40 nm), and they concluded that the labeled bead was not an impeding load for F_1 [24]. In our study, there might be little or no physical effect of the nanocrystals labeling for BR proteins, because we used smaller beads (15–20 nm) than Yasuda's experiment.

In this paper, we demonstrated a method for observing real-time intramolecular dynamics of the 35th amino-acid residue in the *A*-*B* interhelical loop of individual BR molecules in a purple membrane.

The next stage of our research will include monitoring the dynamics of amino residues of loop *F* in BR, which is known to undergo drastic changes while expressing its functions, at a picometer level under physiological conditions and higher experimental speed ($\sim \mu$s) to observe photocycle substeps using DXT.

ACKNOWLEDGMENTS

We would like to thank Dr. N. Yagi (SPring-8/JASRI) for the continuous support for the development of DXT and the staff of BL44B2 beamline in SPring-8 and of Dojindo Lab. for technical support. We also acknowledge Professor Janos K. Lanyi (University of California, Irvine) and Professor Rochard Needleman (Wayne State University) for their suppliances of the BR mutant BR S35C. Y.O. is grateful to the Japan Society for the Promotion of Science for Japanese Junior Scientists for support. The synchrotron radiation experiments were performed at the SPring-8 with the approval of the Japan Synchrotron Radiation Research Institute (JASRI) (Proposal Nos. 2002B0019-NL2-np and 2003A0610-NL-2-np).

[1] S. Weiss, Science **283**, 1676 (1999).
[2] J. M. Thornton, A. E. Todd, D. Milburn, N. Borkakoti, and C. A. Orengo, Nat. Struct. Biol. **7**, 991 (2000).
[3] W. E. Moerner and M. Orrit, Science **283**, 1670 (1999).
[4] P. R. Selvin, Nat. Struct. Biol. **7**, 730 (2000).
[5] Y. C. Sasaki, Y. Suzuki, N. Yagi, S. Adachi, M. Ishibashi, H. Suda, K. Toyota, and M. Yanagihara, Phys. Rev. E **62**, 3843 (2000).
[6] Y. C. Sasaki, Y. Okumura, S. Adachi, Y. Suzuki, and N. Yagi, Nucl. Instrum. Methods Phys. Res. A **467**, 1049 (2001).
[7] Y. C. Sasaki, Y. Okumura, S. Adachi, H. Suda, Y. Taniguchi, and N. Yagi, Phys. Rev. Lett. **87**, 248102 (2001).
[8] T. Oka, H. Kamikubo, F. Tokunaga, J. K. Lanyi, R. Needleman, and M. Kataoka, Photochem. Photobiol. **66**, 768 (1997).
[9] M. Kataoka and H. Kamikubo, Biochim. Biophys. Acta **1460**, 166 (2000).
[10] T. Oka, N. Yagi, T. Fujisawa, H. Kamikubo, F. Tokunaga, and M. Kataoka, Proc. Natl. Acad. Sci. U.S.A. **97**, 14 278 (2000).
[11] A. H. Xie, J. F. Nagle, and R. H. Lozier, Biophys. J. **51**, 627 (1987).
[12] Y. Cao, G. Váró, M. Chang, B. Ni, R. Needleman, and J. K. Lanyi, Biochemistry **30**, 10 972 (1991).
[13] L. S. Brown, G. Váró, R. Needleman, and K. Lanyi, Biophys. J. **69**, 2103 (1995).
[14] S. Adachi *et al.*, Nucl. Instrum. Methods Phys. Res. A **467**, 711 (2001).
[15] Y. Okumura, Y. Taniguchi, and Y. C. Sasaki, J. Appl. Phys. **92**, 7469 (2002).
[16] Y. Okumura, Y. Taniguchi, and Y. C. Sasaki, Thin Solid Films (to be published).
[17] S.-C. Lee, B. D. Yu, D.-Y. Kim, and N. M. Hwang, J. Cryst. Growth **242**, 463 (2002).

[18] K. L. Chopra, J. Appl. Phys. **37**, 3405 (1966).
[19] J. Carlsson, H. Drevin, and R. Axen, Biochem. J. **173**, 723 (1978).
[20] G. Allen and J. I. Harris, Eur. J. Biochem. **62**, 601 (1976).
[21] J. Choi and M. Terazima, Rev. Sci. Instrum. **74**, 319 (2003).
[22] A. Kusumi, Y. Sako, and M. Yamamoto, Biophys. J. **65**, 2021 (1993).
[23] Y. C. Sasaki, Y. Okumura, and N. Oishi (unpublished).
[24] R. Yasuda, H. Noji, M. Yoshida, K. Kinoshita, and H. Itoh, Nature (London) **410**, 898 (2001).
[25] Y. Harada, O. Ohara, A. Takatsuki, H. Itoh, N. Shimamoto, and K. Kinoshita, Nature (London) **409**, 113 (2001).
[26] M. Singh-Zocchim, S. Dixit, V. Ivanov, and G. Zocchi, Proc. Natl. Acad. Sci. U.S.A. **100**, 7605 (2003).